scientific reports

Check for updates

OPEN

Free surface aeration and development dependence in chute flows

Wangru Wei & Jun Deng✉

The microscopic description of the mixture behaviour of air–water flow remains a challenge. It is not clear how to represent a complex two-phase interaction with the turbulent air–water structure development process. In this study, based on the air–water mixing fluctuation properties in self-aerated chute flows, a prediction model of air concentration distribution related to a theoretical transition depth is developed. The air–water turbulent mixing analysis reveals that the mixture flow depth, at which the local air concentration is 0.5, represents the interior transition boundary. The agreement of the calculated results with the test data confirms that local water and air turbulent mixing through the free surface area should be equally considered. On the basis of the interior transition depth, the development of self-aeration mainly manifests as the air turbulent mixing process in the low aerated region, while the water turbulent mixing in the high aerated region remains mostly unchanged. A series of relationships concerning the development of self-aerated flows is proposed to enable quantitative estimations in practical applications of water engineering.

Owing to the high turbulence intensity of free surface flows (Fig. 1), water droplets and air bubbles are key flow structures in self-aerated chute flows, and both air–water mixtures and development processes are important considerations in engineering applications. Understanding the transport mechanisms that govern air–water flow in water release structures has direct implications for natural and industrial processes[1,2]. For air–water mixture flow bulking, the average elevation where the expelled water droplets can reach is of prime importance[3]. For cavitation erosion protection in high-speed open channel flows and air–water transfer of atmospheric gases in natural streams or conduits, the air bubble concentration distribution is of a higher significance because of the net air–water interface area of thousands of tiny bubbles[4,5]. Adequate management of the total dissolved gas requires an accurate prediction of air–water mixture development within the concentration distribution to meet ecosystem demands. Thus, the development of air–water diffusion in high-speed chute flows has received significant attention.

Air–water mixtures were recognized to be a result of their interaction under the turbulence effect. Some similarities between air bubbles and water droplets were observed for a water jet discharging into the atmosphere. Detailed hydrodynamic analyses on the interaction of the air–water surface resulted in a critical condition of free-surface perturbation breakup as a criterion for aeration onset[6]. For engineering purposes, the air–water mixture intensity was commonly described as the air concentration C_a, which was the ratio of air volume to the sum of the air and water volumes. The characterized flow depth y_{90}, where the local $C_a = 0.9$ at the flow cross-section, was widely used as the mixture flow depth to refer to the overall bulk[7,8]. The mixture of water and air parcels resulted in a profile of air concentration distribution in which the air concentration increased from a minimum value at the channel bottom to the free surface. A typical approach for cross-sectional air concentration distributions was an advective–diffusive theory based on air–water mixture levels[9,10]. Valero and Bung[11] extended the analytical application for the air concentration distribution considering outer wave interface effects. Based on air concentration measurements and flow pattern observations of self-aerated open channel flows, researchers analysed the cross-sectional mixture flow on the basis of "layers", such as individual water droplets in air at the upper layer and individual air bubbles in water at the lower layer[12,13]. The transition depth of two layers was defined for which $d^2C_a/dy^2 = 0$ to develop a model to predict air concentration distributions[7]. However, an estimate for the specific depth was not provided, which was affected by several hydraulic conditions. Using a turbulent transport process analysis, the air distribution was logarithmic in the lower layer and was more closely approximated by a

State Key Lab of Hydraulics and Mountain River Engineering, Sichuan University, Chengdu 610065, China. ✉email: djhao2002@scu.edu.cn

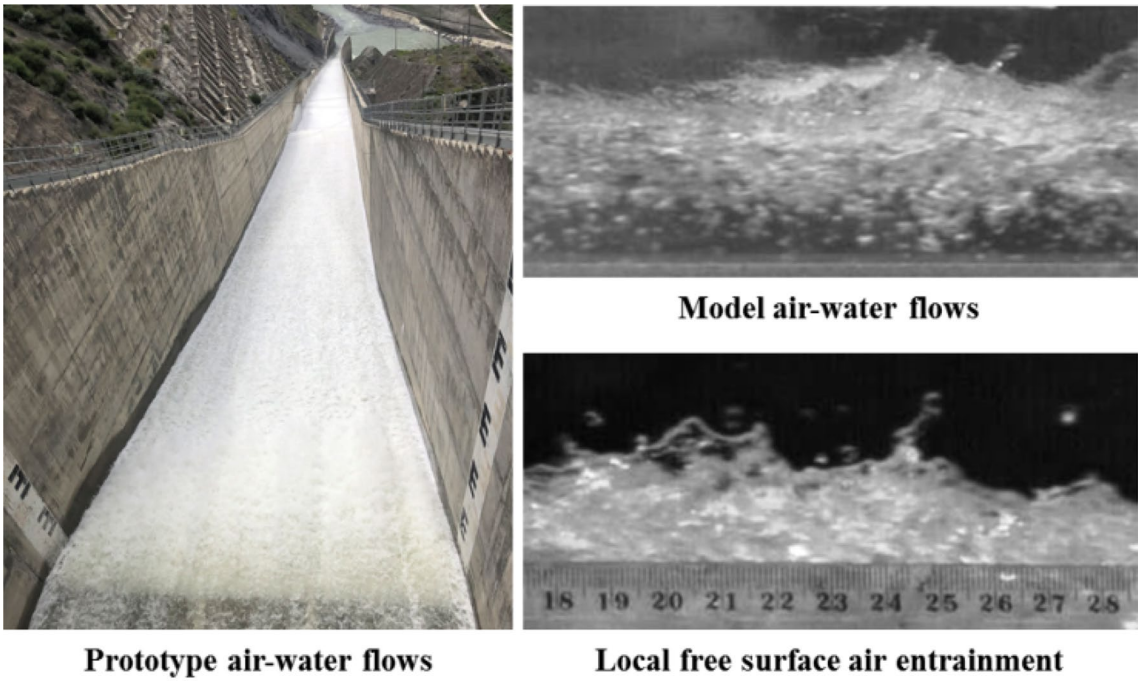

Figure 1. Typical air–water patterns of self-aerated flows in prototype spillways and laboratory models.

cumulative log-normal profile in the upper layer. The conservation equation for the air concentration distribution was developed by characterizing the parcel movement velocity of air bubbles over the entire flow depth[10].

Recently, as measurement and analysis methods for air–water chute flows developed, more detailed characteristics of the mixture flow were investigated[14–16]. For turbulent air–water flows in open channels, the air concentration fluctuation caused by the velocity fluctuation was considered in the air bubble diffusion process of air–water flows. Based on detailed interactions of bubbles with local water in the lower region where $C_a < 0.30$ and the substantial ejections of water droplets in the upper region where $C_a > 0.70$, the intrusive phase-detection measurements highlighted the strong air–water turbulent interactions in the intermediate cross-sectional area where $0.30 < C_a < 0.70$[17,18]. According to the definition of air concentration in air–water flows, the quantities of water and air are equal if the local $C_a = 0.50$. The specific flow depth y_{50}, where $C_a = 0.50$, can be considered canonically to undergo a transition from bubbly flow to droplet flow in the cross-section. Basic theoretical analyses confirmed that the specific flow depth y_{50} can be used as a hypothesis condition to describe the air concentration distribution of self-aerated open channel flows[19,20]. It can be deduced that owing to the difference in the air–water structures at different layers of the flow cross-section, there must be an interior transition flow depth that can represent the detailed air–water structure development.

However, despite the key role of the interior transition depth in the air–water turbulent mixing process, theoretical verifications concerning the specific transition depth in self-aerated open channel flows are limited. Little information about the effect of particle turbulence on the average air concentration distribution in self-aerated flows is available. This study focuses on the air–water mixing affected by turbulence to analyse the theoretical transition depth in self-aerated chute flows. The prediction of the air concentration distribution from the transition depth represents the first attempt to verify the rationality of the interior transition depth. Moreover, this study provides further insights into air–water development differentiated by the transition depth of self-aerated flows, aiming to propose quantitative estimations in practical applications.

Concentration and density fluctuations in turbulent air–water flows

For a time average air–water control volume, the volume of the control mixture parcel is V_0, which is equal to the product of the unit area A_0 and the displacement distance per unit time. The time average air and water concentrations of the control mixture parcel are defined as $C_{a0} = V_a/V_0$ and $C_{w0} = V_w/V_0$, respectively. The time average density of the control mixture volume is ρ_{m0}. The mass of the mixture volume M_0 is defined as $M_0 = \rho_{m0} V_0$, where V_0 is the time average volume equal to $V_a + V_w$. For turbulent air–water flows, the time average parameter is a decomposition result as the sum of the time average mean factor and the time average fluctuation factor. To retain ρ_{m0}, it is hypothesized that the value of M_0 is approximately equal to

$$M_0 \approx \rho_{m0} C_{a0} V_0 + \rho_{m0} C_{w0} V_0 \quad (1)$$

The two terms can be considered as the mass rate of air contribution $M_a = \rho_{m0} C_{a0} V_0$ and mass rate of water contribution $M_w = \rho_{m0} C_{w0} V_0$. In self-aerated open channel flows, there are two basic transportation patterns in the y-direction perpendicular to the streamwise direction, that is, the air phase and water phase transportations. If it is considered that the mixture fluid crosses the unit area per time, the two terms become $\rho_{m0} C_{a0} u_a^*$ and $\rho_{m0} C_{w0} u_w^*$,

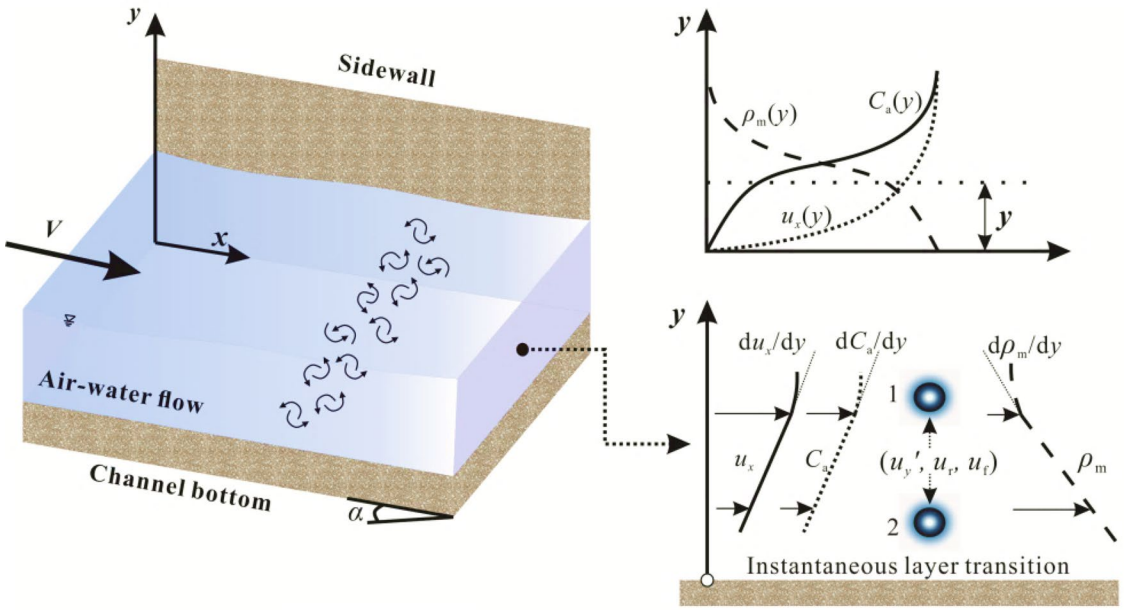

Figure 2. Schematic definitions for the turbulence fluctuations of air–water mixture parcels (α is the channel slope).

where u_a^* and u_w^* are two characteristic velocities, representing the transition of the control volume. They consist of the turbulent eddy fluctuation velocity u_y', droplet falling-back velocity u_f and air bubble rising velocity u_r.

The definition of the characterized air–water volume is related to the fully developed two-phase flow on the basis of the mixing length theory[21]. The air–water transfer occurs under a uniform air–water mixture, and the air–water flow behaves as a homogeneous mixture across the flow section[22,23]. This ensures sufficient time-average air–water control volumes for flow property analyses. Both of them are the interaction of turbulence fluctuation and gravity or buoyancy forces, resulting in volume concentration and density changes. The time average fluctuation air concentration shows an important role in drag reduction, and the production of a negative turbulent shear stress component is obtained using momentum conservation analysis[24,25]. This indicates that the air bubble interfacial transfer for the unit air–water control volume requires vital attention and that the time-average fluctuation air concentration affected by the fluctuation velocity can be used as a component part of the turbulent air–water control volume. For flow density properties, the mass transfer among air–water control particles is the accompanying appearance causing the time average fluctuation of unit volume density. The mass transfer intensity is significantly correlated with local eddy shear, fluctuation, bubble and air–water surface transfer effects in open channel turbulent flows[26–29]. For an average air–water control volume with a constant concentration, more bubbles with smaller size can significantly raise the specific surface area, compared to less bubbles with larger bubble size dominant condition. General turbulent models are established based on the microscopic air–water mass transfer and bubble density and size variations[30–32]. Thus, the density variation of the control volume should be considered due to microscopic air–water structures. In the present study, the deviation of the local time average mean density of air–water control particles is the time average fluctuation of particle density. The effect of the time average fluctuation of particle density is among air–water control particles, and the entire air–water mass is constant with the conservation of mass. The time-average fluctuation density affected by the flow turbulence and fluctuation factors can be used as a component part of the turbulent air–water control volume. Consequently, for air and water diffusion generalizations, the approach of mean and fluctuating decompositions for the air concentration and mixture density is used in turbulent self-aerated chute flows.

Prandtl's mixing length theory is introduced to hypothesize the time-average mean and fluctuation for concentration and density properties, which are determined by the exchange on a macroscale analogous to that of molecular motion[21]. Figure 2 schematically shows an air–water mixture volume transition between layer 1 and layer 2 affected by the characteristic velocities. For example, due to u_y' in the $-y$ direction, the density and air concentration of the air–water mixture volume at level 1 are retained when it just arrives at level 2, and the density and air concentration at level 2 decrease soon after by exchanging with the flow in the neighbourhood of level 2. The detailed air–water property fluctuations are shown in Table 1, where the time-average and fluctuation local densities are ρ_m and ρ_m'; the time-average mean and fluctuation water droplet concentration and C_w and C_w'; the time-average mean and fluctuation air bubble concentration are C_a and C_a'. In the vertical direction (y), the air–water mixture volume is presumed to retain its original time-averaged properties at the arrival position, including velocity, density, and concentration[33–35]. Thus, the vertical density and air concentration fluctuations of the air–water mixture parcel through level 1 are given by $\rho_m' < 0$ and $C_a' > 0$, respectively. Based on these definitions for density and air concentration fluctuations of air–water mixture volumes, it is deduced that both the density and air concentration fluctuations are caused by the turbulent motion of mixture parcels. For other factors, u_f and u_r, there are different exchange motion processes analogous to the turbulent eddy effect. The relationship

Parameters	Density		Concentration	
$u_y' > 0$	$\rho_m' > 0$	$\rho_{m0} = \rho_m + \rho_m'$	$C_w' > 0$	$C_{w0} = C_w + C_w'$
$u_y' < 0$	$\rho_m' < 0$	$\rho_{m0} = \rho_m - \rho_m'$	$C_a' > 0$	$C_{a0} = C_a + C_a'$
$u_r > 0$	$\rho_m' > 0$	$\rho_{m0} = \rho_m + \rho_m'$	$C_a' < 0$	$C_{a0} = C_a - C_a'$
$u_f < 0$	$\rho_m' < 0$	$\rho_{m0} = \rho_m - \rho_m'$	$C_w' < 0$	$C_{w0} = C_w - C_w'$

Table 1. Fluctuation properties in the air–water mixing process.

between the time-average concentration and mixture flow density[7] is $\rho_{m0} \approx \rho_{w0}\,(1 - C_{a0}) = \rho_{w0} C_{w0}$, where ρ_{w0} is the water density. Considering this related expression, the fluctuation density of the air–water mixture volume is

$$\rho_m' = \rho_w(1 - C_{a0}) - \rho_w(1 - C_a) = -\rho_w C_a' \tag{2}$$

In the present study, the mixture of air and water can be approximated as two diffusion processes, that is, the air mixing process and water mixing process. Thus, the time-average mean and fluctuation for concentration and density properties are treated, respectively.

All results are presented at normal temperatures and standard atmospheric pressure conditions. The free surface aeration and air–water mixture processes are determined by the free surface air entrainment capacity and flow turbulence intensity. Uniform equilibrium air–water flows are defined as the air concentration distribution independent of the streamwise direction. The fully aeration condition means the cross-sectional fully air diffusion across the flow section without the clear water layer existence. Detailed descriptions of the two turbulent mixing processes combined with multiple fluctuation properties are shown in the following sections.

Air turbulent mixing

The time average mass flux of air contribution m_{a1} per unit area transported by the local turbulent fluctuation u_{y1}' in the $-y$-direction is

$$m_{a1} = (\rho_m - \rho_m') \cdot (C_a + C_a') \cdot u_{y1}' = \rho_m C_a u_{y1}' + \rho_m C_a' u_{y1}' - C_a \rho_m' u_{y1}' - \rho_m' C_a' u_{y1}' \tag{3}$$

The terms $C_a' u_{y1}'$ and $\rho_m' u_{y1}'$ are considered turbulent diffusion rates affected by the air phase. The turbulent diffusion processes for both the air concentration and mixture density are identical, which are analogous to the Boussinesq hypothesis[31]. They are proportional to the gradient of the time-average concentration, given by

$$C_a' u_{y1}' = K_{a1} \frac{dC_a}{dy} \tag{4}$$

$$\rho_m' u_{y1}' = -K_{a1} \frac{d\rho_m}{dy} \tag{5}$$

where K_{a1} is a characterized turbulent diffusion coefficient. For steady flow in an open channel, Eq. (3) yields

$$\overline{m_{a1}} = \rho_m K_{a1} \frac{dC_a}{dy} + C_a K_{a1} \frac{d\rho_m}{dy} - \overline{\rho_m' C_a' u_{y1}'} = (1 - 2C_a)\rho_w K_{a1} \frac{dC_a}{dy} - \overline{\rho_m' C_a' u_{y1}'} \tag{6}$$

The time average mass flux of air contribution m_{a2} rising up owing to the buoyancy effect u_r in the $+y$-direction is

$$m_{a2} = (\rho_m + \rho_m') \cdot (C_a - C_a') \cdot u_r \cos\alpha = \rho_m C_a u_r \cos\alpha - \rho_m C_a' u_r \cos\alpha + C_a \rho_m' u_r \cos\alpha - \rho_m' C_a' u_r \cos\alpha \tag{7}$$

The terms $C_a' u_r \cos\alpha$ and $\rho_m' u_r \cos\alpha$ are considered the diffusion rates by the buoyancy effect, given by

$$C_a' u_r \cos\alpha = K_{a2} \frac{dC_a}{dy} \tag{8}$$

$$\rho_m' u_r \cos\alpha = -K_{a2} \frac{d\rho_m}{dy} \tag{9}$$

where K_{a2} is the diffusion coefficient affected by the buoyancy. For steady flow in an open channel, Eq. (7) yields

$$\overline{m_{a2}} = \rho_w (1 - C_a) C_a u_r \cos\alpha - \rho_w K_{a2} (1 - 2C_a) \frac{dC_a}{dy} - \overline{\rho_m' C_a'} u_r \cos\alpha \tag{10}$$

For uniform mixing of air in the water, the mass flux of air entrained in the $-y$-direction equals that of air rising in the $+y$-direction, that is,

$$\overline{m_{a1}}=\overline{m_{a2}} \tag{11}$$

Then, it is obtained as

$$(1-2C_a)(K_{a1}+K_{a2})\frac{dC_a}{dy}=(1-C_a)C_a u_r\cos\alpha+\frac{\overline{\rho'_m C'_a u'_{y1}}-\overline{\rho'_m C'_a}u_r\cos\alpha}{\rho_w} \tag{12}$$

Considering that the flow density fluctuation ρ_m' is much smaller than the water density ρ_w, that is, $\rho_m' << \rho_w$, and the higher order of multiple ρ_m'C_a'u_y' and ρ_m'C_a'$u_r\cos\alpha$, the second term on the right term is neglected, that is,

$$(1-2C_a)(K_{a1}+K_{a2})\frac{dC_a}{dy}=(1-C_a)C_a u_r\cos\alpha \tag{13}$$

It should be noted that in the right term, $(1-C_a)C_a u_r\cos\alpha>0$, and in the left term, $K_{a1}+K_{a2}>0$ and $dC_a/dy>0$. The case for which the air phase continues to diffuse during the turbulent mixing process is given by the condition that the sign of the left term is positive; that is, $C_a<0.5$ should be maintained to ensure that Eq. (13) is satisfied. This indicates that based on the air mixing process under the turbulent diffusion effect, the limiting air concentration is $C_a<0.5$.

The alternative formulation for the final rising velocity of air parcel under a local concentration condition is introduced: $u_r=(u_r)_0(1-C_a)^2$, where $(u_r)_0$ is the final velocity of an individual air parcel in pure water[36]. This is a generalized expression that assumes that the control volume movement is affected by mixture flow density variation and does not interact with each other. A dimensionless air turbulent diffusivity K_a and a dimensionless distance y^* are normalized by a flow depth y_{50}, where local $C_a=0.5$, given as

$$K_a=\frac{y_{50}(u_r)_0\cos\alpha}{K_{a1}+K_{a2}},\quad y^*=\frac{y}{y_{50}} \tag{14}$$

Then, Eq. (13) yields

$$\frac{1-2C_a}{C_a(1-C_a)^3}\frac{dC_a}{dy^*}=K_a \tag{15}$$

Integrating Eq. (15) in the y-direction yields

$$\frac{1}{1-C_a}-\ln\frac{1-C_a}{C_a}-\frac{1}{2(1-C_a)^2}=K_a y^*+D_a \tag{16}$$

where D_a is the integration constant. This relation is a function of the air concentration distribution in the region where $C_a\le 0.5$. The relationship between K_a and D_a can be deduced from $C_a=0.5$ for $y^*=1$, that is,

$$K_a+D_a=0 \tag{17}$$

Water turbulent mixing

The time average mass flux of water contribution m_{w1} per unit area transported by the local turbulent fluctuation u_{y2}' in the $+y$-direction is

$$m_{w1}=(\rho_m+\rho'_m)\cdot(C_w+C'_w)\cdot u'_{y2}=\rho_m C_w u'_{y2}+\rho_m C'_w u'_{y2}+C_w\rho'_m u'_{y2}+\rho'_m C'_w u'_{y2} \tag{18}$$

The terms C_w'u_{y2}' and ρ_m'u_{y2}' are considered the turbulent diffusion rate affected by the water phase. The turbulent diffusion processes for both the water concentration and mixture density are identical, and they are proportional to the gradient of the time-average concentration, given by

$$C'_w u'_{y2}=-K_{w1}\frac{dC_w}{dy} \tag{19}$$

$$\rho'_m u'_{y2}=-K_{w1}\frac{d\rho_m}{dy} \tag{20}$$

where K_{w1} is a turbulent diffusion coefficient. For steady flow in an open channel, Eq. (18) yields

$$\overline{m_{w1}}=-2\rho_w C_w K_{w1}\frac{dC_w}{dy}+\overline{\rho'_m C'_a u'_{y2}} \tag{21}$$

The time average mass flux of water contribution m_{w2} falling back owing to the gravity effect in the $-y$-direction u_f is

$$m'_{w2}=(\rho_m-\rho'_m)\cdot(C_w-C'_w)\cdot u_f\cos\alpha=\rho_m C_w u_f\cos\alpha-\rho_m C'_w u_f\cos\alpha-C_w\rho'_m u_f\cos\alpha+\rho'_m C'_w u_f\cos\alpha \tag{22}$$

The terms C_w'$u_f\cos\alpha$ and ρ_m'$u_f\cos\alpha$ are considered the diffusion rates by the gravity effect, given by

$$C'_{\mathrm{w}} u_{\mathrm{f}} \cos\alpha = -K_{\mathrm{w2}} \frac{\mathrm{d}C_{\mathrm{w}}}{\mathrm{d}y} \tag{23}$$

$$\rho'_{\mathrm{m}} u_{\mathrm{f}} \cos\alpha = -K_{\mathrm{w2}} \frac{\mathrm{d}\rho_{\mathrm{m}}}{\mathrm{d}y} \tag{24}$$

where K_{w2} is a diffusion coefficient affected by gravity. For steady flow in an open channel, Eq. (22) yields

$$\overline{m_{\mathrm{w2}}} = C_{\mathrm{w}}^2 \rho_{\mathrm{w}} u_{\mathrm{f}} \cos\alpha + 2\rho_{\mathrm{w}} C_{\mathrm{w}} K_{2\mathrm{w}} \frac{\mathrm{d}C_{\mathrm{w}}}{\mathrm{d}y} + \overline{\rho'_{\mathrm{m}} C'_{\mathrm{w}}} u_{\mathrm{f}} \cos\alpha \tag{25}$$

For uniform mixing of water in the air, the mass flux of the water contribution expelled in the $+y$-direction equals that falling back in the $-y$-direction, that is,

$$\overline{m_{\mathrm{w1}}} = \overline{m_{\mathrm{w2}}} \tag{26}$$

Then, it is obtained as

$$-2C_{\mathrm{w}}(K_{\mathrm{w1}} + K_{2\mathrm{w}}) \frac{\mathrm{d}C_{\mathrm{w}}}{\mathrm{d}y} = C_{\mathrm{w}}^2 u_{\mathrm{f}} \cos\alpha + \frac{\overline{\rho'_{\mathrm{m}} C'_{\mathrm{w}}} u_{\mathrm{f}} \cos\alpha - \overline{\rho'_{\mathrm{m}} C'_{\mathrm{a}} u'_{y2}}}{\rho_{\mathrm{w}}} \tag{27}$$

This is analogous to the previous analysis; the second term on the right term is neglected, that is,

$$-2C_{\mathrm{w}}(K_{\mathrm{w1}} + K_{2\mathrm{w}}) \frac{\mathrm{d}C_{\mathrm{w}}}{\mathrm{d}y} = C_{\mathrm{w}}^2 u_{\mathrm{f}} \cos\alpha \tag{28}$$

The alternative velocity formulation for the local concentration condition in the mixture fluid is introduced as $u_{\mathrm{f}} = (u_{\mathrm{f}})_0 (1 - C_{\mathrm{w}})^2$, where $(u_{\mathrm{f}})_0$ is the final velocity of an individual water parcel. A dimensionless turbulent diffusivity K_{w} is defined as

$$K_{\mathrm{w}} = \frac{y_{50} (u_{\mathrm{f}})_0 \cos\alpha}{K_{\mathrm{w1}} + K_{\mathrm{w2}}} \tag{29}$$

Then, Eq. (28) with the dimensionless y^* yields

$$\frac{-2}{C_{\mathrm{w}}(1 - C_{\mathrm{w}})^2} \frac{\mathrm{d}C_{\mathrm{w}}}{\mathrm{d}y^*} = K_{\mathrm{w}} \tag{30}$$

Integrating Eq. (30) in the y-direction yields

$$2\left(\ln \frac{1 - C_{\mathrm{w}}}{C_{\mathrm{w}}} - \frac{1}{1 - C_{\mathrm{w}}} \right) = K_{\mathrm{w}} y^* + D_{\mathrm{w}} \tag{31}$$

where D_{w} is the integration constant. This relation is a function of the water concentration distribution. The air concentration distribution can be obtained by $C_{\mathrm{a}} = 1 - C_{\mathrm{w}}$, that is,

$$2\left(\ln \frac{C_{\mathrm{a}}}{1 - C_{\mathrm{a}}} - \frac{1}{C_{\mathrm{a}}} \right) = K_{\mathrm{w}} y^* + D_{\mathrm{w}} \tag{32}$$

Considering y_{90} as the total mixture flow depth where the local water droplet concentration is $C_{\mathrm{w}} = 0.1$ (and $C_{\mathrm{a}} = 0.9$), the relationship between K_{w} and D_{w} can be deduced under two boundary conditions: $C_{\mathrm{w}} = 0.5$ for $y^* = 1$ and $C_{\mathrm{w}} = 0.1$ for $y^* = y_{90}/y_{50}$, which yields

$$K_{\mathrm{w}} = \frac{6.172}{y_{90}/y_{50} - 1}, \quad D_{\mathrm{w}} = -4 - K_{\mathrm{w}} \tag{33}$$

Comparing the air and water turbulent mixing Eqs. (15) and (30), it is found that the concentration gradient variation is continuous for the water phase, while it is not continuous for the air phase in air–water flows. Thus, this theoretical analysis reveals that y_{50}, where $C_{\mathrm{a}} = 0.5$, represents the interior boundary for air turbulent mixing and water turbulent mixing in which the water phase can be considered a homogenous phase.

Air concentration distributions

The turbulent diffusion coefficients K_{a} and K_{w} are determined by the relationship between the aeration level and y_{50}/y_{90}. The average cross-sectional air concentration C_{mean} is defined as the integration of the local C_{a} over the mixture flow depth between the channel bottom at $y = 0$ and y_{90}:

$$C_{\mathrm{mean}} = \frac{1}{y_{90}} \int_{y=0}^{y=y_{90}} C(y) \mathrm{d}y \tag{34}$$

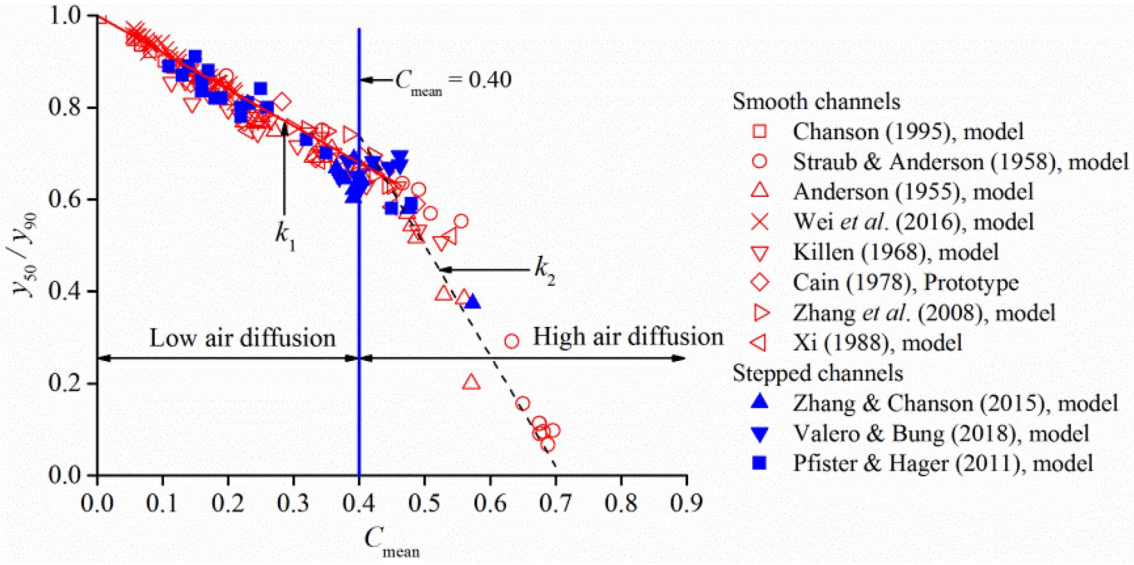

Figure 3. The variation of y_{50}/y_{90} with the increase of C_{mean} in self-aerated open channel flows.

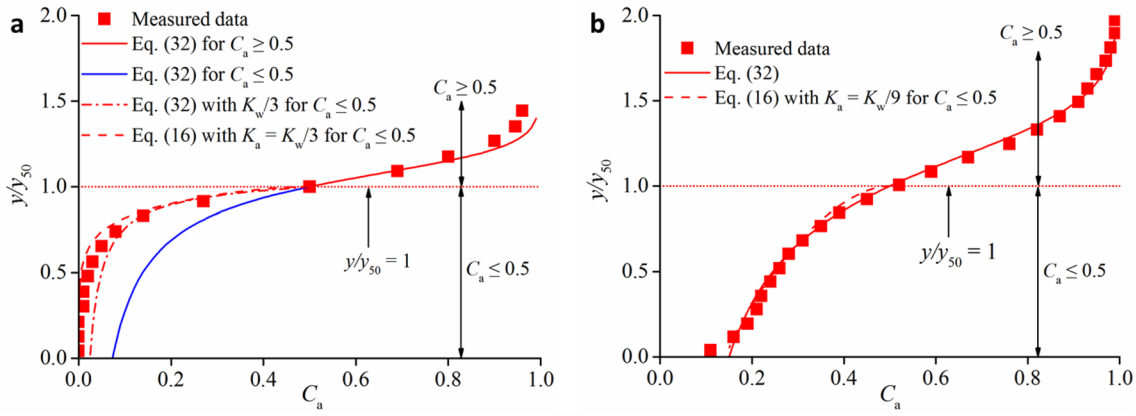

Figure 4. Air concentration distribution for fully and partially aerated diffusions: (**a**) $C_{mean} = 0.23$, (**b**) $C_{mean} = 0.43$.

The statistical relationships between y_{50}/y_{90} and C_{mean} are shown in Fig. 3 for different model and prototype chute flows. For a constant channel slope condition, y_{50}/y_{90} decreases with increasing C_{mean}, and it is independent of other hydraulic conditions, such as approach flow conditions, smooth or stepped channel type, and slope. For C_{mean} values smaller than approximately 0.40, a linear trend is followed with a constant gradient $k_1 \approx -0.8$. The gradient changes to $k_2 \approx -2.4$ for C_{mean} greater than approximately 0.40, for which the mixture flow cross-section is fully aerated and the local air concentration is greater than 0.10. On the basis of $C_{mean} = 0.40$, the two relationships can be expressed as $y_{50}/y_{90} = 1–0.8C_{mean}$ for $C_{mean} < 0.40$ and $y_{50}/y_{90} = 1.7–2.4C_{mean}$ for $C_{mean} > 0.40$. This indicates that the interior transition boundary of turbulence diffusion changes suddenly if the aeration development of the flow cross-section exceeds $C_{mean} = 0.40$.

As aeration develops through the turbulent free surface, the air–water mixing layer diffuses into the water flow, protruding to the channel bottom. For some cases, the entire flow is partially aerated, where a clear water layer exists at the bottom area of the entire flow. For the other cases, the entire flow section becomes fully aerated without the presence of clear water. Here, the air concentration distributions obtained from the prototype Aviemore dam spillway[37] are used for detailed analysis. For partially aerated flows, the measured data showed that the local C_a at the bottom area was mostly smaller than 0.05 for $C_{mean} < 0.40$. If K_w and D_w are obtained from Eq. (33), the comparison between the measured data and Eq. (32) in Fig. 4a shows that the theoretical prediction is acceptable only for $C_a > 0.5$, while for $C_a < 0.5$, Eq. (32) overestimates the air diffusion in the low aerated region. This indicates that the presence of a clear water layer can reduce the air bubble penetration caused by water turbulent diffusion. For this case, it is suggested that $K_a = K_w/3$. For fully aerated flows, the local C_a mainly exceeds 0.10 at the channel bottom when C_{mean} exceeds 0.40. The determinations of K_w and D_w are obtained from Eq. (33). The comparison between the measured data and Eq. (32) is shown in Fig. 4b. The good agreement indicates that homogenous water turbulent mixing in self-aerated open channel flows can predict the air concentration distribution for both high aerated regions ($C_a > 0.5$) and low aerated regions ($C_a < 0.5$). Under this situation, the

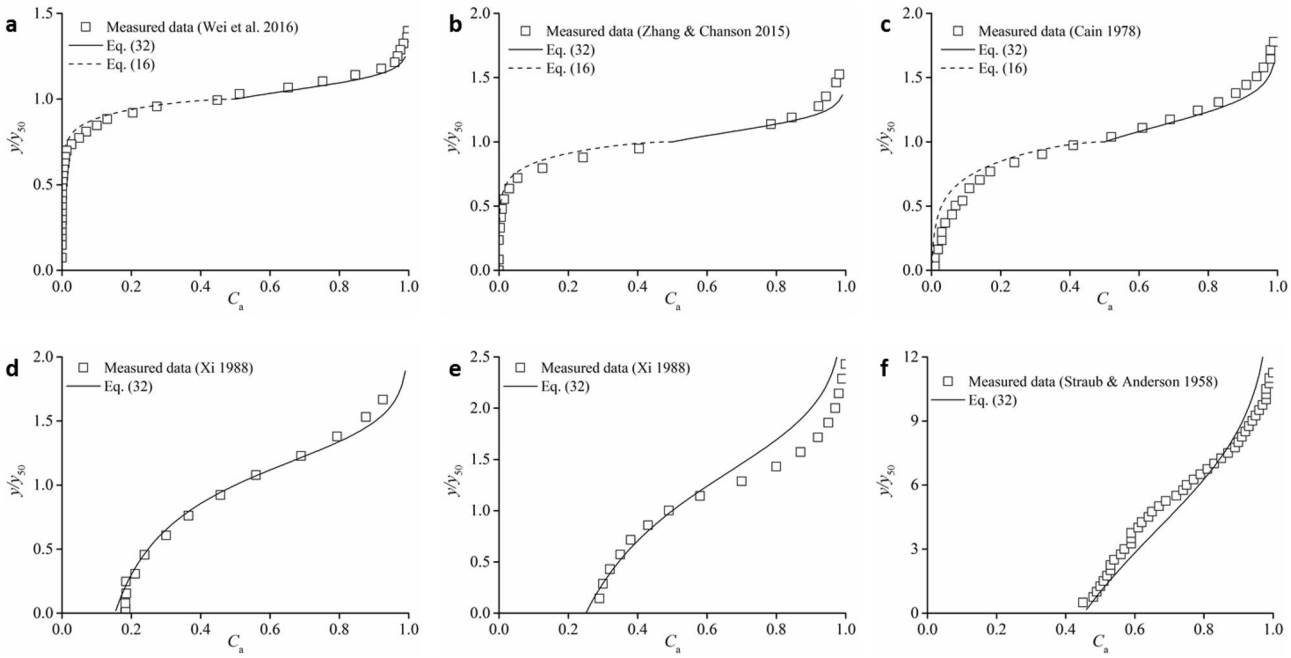

Figure 5. Comparison of calculated C_a profiles with the measured air concentration distribution in self-aerated open channel flows. (**a**) $C_{mean} = 0.15$ (smooth channel). (**b**) $C_{mean} = 0.21$ (stepped channel). (**c**) $C_{mean} = 0.32$ (smooth channel). (**d**) $C_{mean} = 0.41$ (smooth channel). (**e**) $C_{mean} = 0.54$ (smooth channel). (**f**) $C_{mean} = 0.65$ (smooth channel).

sudden change in y_{50}/y_{90} represents the difference in interior boundary variation and the capacity reduction of air diffusion for $C_{mean} < 0.40$. Because the ratio of $k_1/k_2 = 1/3$, K_w needs to be three times greater. The air turbulent diffusivity K_a can be set as $K_a = K_w/9$ to obtain good agreement on the air concentration distribution in the low aerated region ($C_a < 0.5$). Consequently, the characterized flow depth y_{50}, at which the local air concentration is 0.5, represents the interior transition boundary in self-aerated flows $C_{mean} < 0.40$, and the air–water mixture cross-section can be divided into water turbulent mixing and air turbulent mixing. For $C_{mean} > 0.40$, the full cross-section can be seen as the water mixing process, and the $y < y_{50}$ region also fits the air turbulent mixing process.

Based on Eqs. (16) and (32) with boundary conditions, the calculated air concentration profiles are compared with the experimental and prototype data[12,20,37–39], as shown in Fig. 5. For each case, the determinations of K_w and K_a are deduced from each C_{mean} within the calibrated procedure proposed above. For $C_{mean} < 0.40$ within clear water, the air concentration distributions agree well for air and water turbulent mixing areas, and the theoretical results are applicable for both smooth and stepped spillways. Thus, it is reasonable to relate the diffusion behaviour of air turbulent mixing with water turbulent mixing. Air diffusion within the presence of clear water is verified to change K_a and restrain air diffusion according to the sudden change in the y_{90}/y_{50} gradient for $C_{mean} \approx 0.40$. Moreover, the air concentration profiles for high C_{mean} up to 0.65 agree with the theoretical results obtained from water turbulent mixing. This indicates that the local water turbulent mixing in the free-surface area plays an important role in the air–water mixture process. The air–water structures in the upper spray region, where macroscopic water roughness and microscopic water particles are predominant, are of various types, such as individual droplets, water projections, mixture clusters, and foam transported with the free surface. Owing to the individual water structures affected by the interaction between the free surface and the local turbulence, the satisfactory predicted results indicate that the movement of complex water-predominant structures can be simplified as local individual water particle movements affected by turbulence.

Most theoretical and observation descriptions of the aerated region of classical air–water mixtures in self-aerated flows involve a "layered" description: (1) individual water droplets in air in the top layer; (2) a mixture of water and air in the middle layer; and (3) individual air bubbles in water in the bottom layer. The layer is a generalization concept on the basis of the dominant air–water structures. In the present theoretical derivation process, there is no flow depth limit until the discussion of the satisfied condition for establishing the equation. The specific interior flow depth y_{50} is obtained because the boundary condition of particle concentration is 0.5 in the air or water mixing process affected by turbulent diffusion. The interior transition depth y_{50} is considered the transition layer from the top layer, where the water phase dominates, to the bottom layer, where the effect of the air phase increases. Consequently, the characterized water parcels and air parcels should be considered equally in high-speed chute flows, and the movement of complex air–water structures can be simplified as local particle turbulent diffusion. This promotes the further understanding and description of layer theory in self-aerated open channel flows.

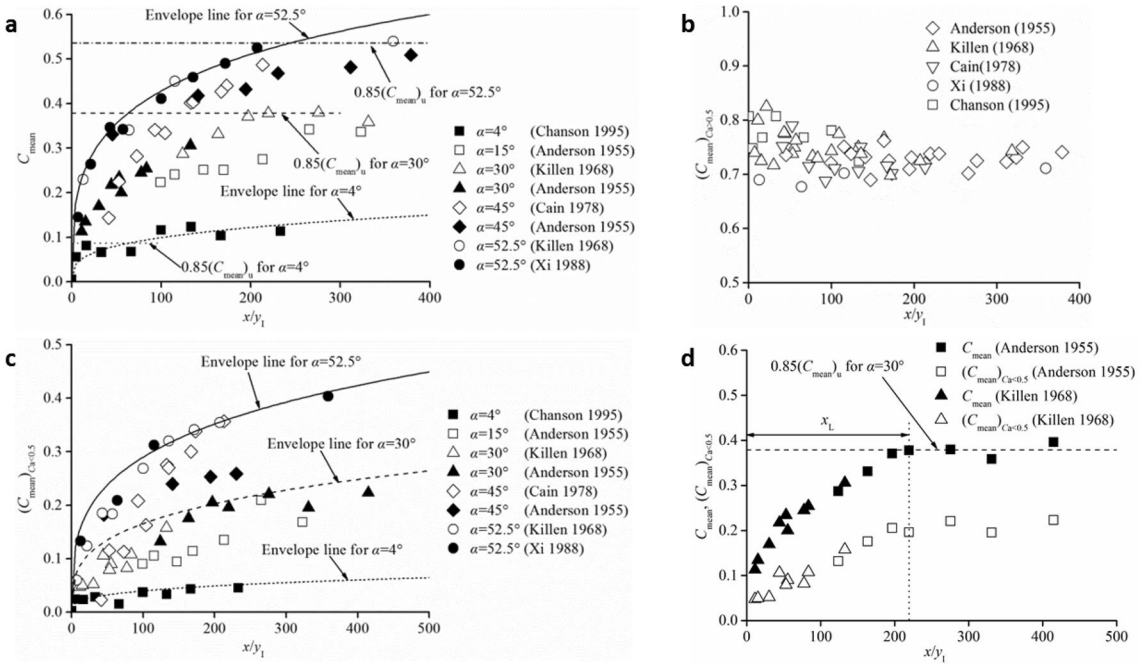

Figure 6. Typical self-aeration characteristics in the streamwise development process. (**a**) C_{mean}. (**b**) $(C_{mean})_{Ca>0.5}$. (**c**) $(C_{mean})_{Ca<0.5}$. (**d**) Comparison of the developmental processes between C_{mean} and $(C_{mean})_{Ca<0.5}$.

Self-aeration streamwise development

When self-aeration of the free surface occurs in high-speed chute flows, the air–water mixes with an increase in the macroscopic C_{mean}, as shown in Fig. 6a, where x is the distance from the self-aeration inception point along the streamwise direction, and y_I is the initial water flow depth at the inception point. x/y_I is used as the nondimensional parameter to illustrate the development of self-aerated flows. The water flow discharge per unit width ranges from 0.15 to 3.16 m^2/s with $\alpha = 4°–52.5°$[40–43]. Owing to the differences between water and air turbulent mixing areas, the mean cross-sectional air concentration can be divided into two parts demarcated by y_{50}, separately defined as $(C_{mean})_{Ca>0.5}$ and $(C_{mean})_{Ca<0.5}$:

$$(C_{mean})_{Ca>0.5} = \frac{1}{y_{90} - y_{50}} \int_{y_{50}}^{y_{90}} C_a dy, \quad y > y_{50} \tag{35}$$

$$(C_{mean})_{Ca<0.5} = \frac{1}{y_{50}} \int_{0}^{y_{50}} C_a dy, \quad y < y_{50} \tag{36}$$

In Fig. 6b, the values of $(C_{mean})_{Ca>0.5}$ do not change notably in the entire development process, remaining at $(C_{mean})_{Ca>0.5} \approx 0.75$ in the incipient distance for $0 < x/y_I < 50$ and slightly changing to $(C_{mean})_{Ca>0.5} \approx 0.70$ for $x/y_I > 50$. The development of $(C_{mean})_{Ca<0.5}$ is similar to the variation in C_{mean} as self-aeration develops downstream (Fig. 6c). This is because the air concentration in the upper free-surface area results from the growth of surface waves and entrapped air, which develops rapidly into small free-surface roughness and water droplets in the following incipient distance[4]. Altogether, once self-aeration occurs, the local water turbulent mixing affected by the free-surface turbulence is relatively stable. The development of an air–water mixture in a self-aerated open channel flow manifests mainly as air diffusion in the water. Compared with the two developments of C_{mean} and $(C_{mean})_{Ca<0.5}$ with other identical conditions in Fig. 6d, the approximately same trends confirm that as the air turbulent mixing approaches near full development, the entire air–water mixture of self-aerated flows reaches a uniform equilibrium level.

Furthermore, self-aeration typically reaches the near-fully developed region with an approximately identical development process under the same channel slope conditions, such as $\alpha = 30°$, 45° and 52.5°, as shown in Fig. 6a and Fig. 6d. For uniform air–water mixture flow conditions, the mean cross-sectional air concentration $(C_{mean})_u$ is dependent only on the channel slope. Hager[4] analyzed the uniform $(C_{mean})_u$ for $7.5° \le \alpha \le 75°$ and defined it as

$$(C_{mean})_u = 0.75(\sin\alpha)^{0.75} \tag{37}$$

This equation results in $(C_{mean})_u$ being approximately 0.7 for a steep channel slope $\alpha = 75°$, and it is in agreement with the y_{50}/y_{90} variation within C_{mean}. This indicates that y_{50}/y_{90} decreases to zero for extremely developed aeration near $C_{mean} = 0.7$. In the present analysis, it is considered that the air–water flow reaches a near-fully developed region when $C_{mean} \ge 0.85(C_{mean})_u$ (reference lines in Fig. 6a), owing to differences in the experimental

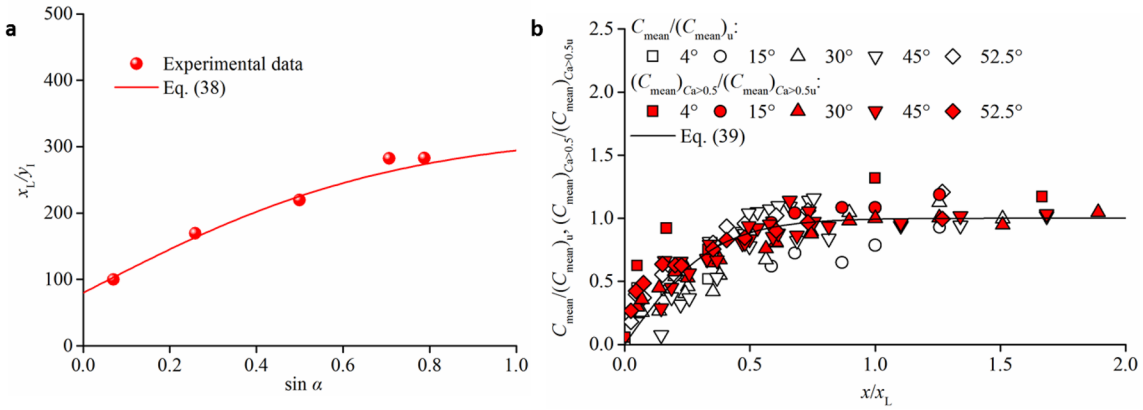

Figure 7. Relationships between self-aeration and development distance length. (**a**) effect of α on x_L. (**b**) Variations in C_{mean} and $(C_{mean})_{Ca<0.5}$ in the self-aeration development distance.

measurement. The streamwise distance length x_L from the inception point to the fully developed flow cross-section is defined as the self-aeration development length, as shown in Fig. 6d. For a specific channel slope condition, the average value is used, which is deduced from the experimental data. A larger channel slope corresponds to a longer distance of self-aeration development. In Fig. 7a, the relationship between x_L/y_I and sinα can be expressed as

$$\frac{x_L}{y_I} = 280 \cdot \tanh(1.2 \sin \alpha) + 80 \tag{38}$$

The developments of C_{mean} and $(C_{mean})_{Ca<0.5}$ can be applied as

$$\frac{C_{mean}}{(C_{mean})_u} = \frac{(C_{mean})_{Ca<0.5}}{(C_{mean})_{Ca<0.5u}} = \tanh\left(2.8\frac{x}{x_L}\right) \tag{39}$$

where $(C_{mean})_{Ca<0.5u}$ is the mean cross-sectional air concentration in the air turbulent mixing area ($y < y_{50}$) for the fully developed uniform region. The streamwise normalization of Eq. (39) includes x/x_L. Figure 7b compares all datasets with the data pertaining to Eq. (39), resulting in a coefficient of determination $R^2 = 0.847$. The data trend indicates that self-aeration in high-speed chute flows develops rapidly in the incipient half of the streamwise distance length $x/x_L < 0.5$ and reduces gradually until the air–water uniform condition is reached. As Eqs. (38) and (39) describe C_{mean} using y_I and these relationships in self-aerated chute flows can be estimated for a given initial configuration, it is expected that the quantitative expressions are comparable for both model and prototype applications.

The present study proposes an analysis of air–water turbulent diffusion based on a theoretical model. Recent experimental and theoretical analyses confirm that a reasonable model for particle groups in air–water flows can result in reliable two-phase properties, including time-average mixture-velocity and air concentration distributions[44]. According to the present analysis results, the air–water mixture in high-speed chute flows is a result of the interaction of air and water under turbulence. Microscopic water and air turbulent mixing through the free surface plays an important role in air–water flow development. Further research on self-aeration onset should consider the formation of water ejection and air entrainment equally. The detailed differences in water ejection and air entrainment are required for a complete understanding of air–water mixture development, thereby helping promote hydraulic and environmental applications. Moreover, the effects of individual particle distribution and movement in different flow conditions, including flow turbulence intensity and mixture levels, should be further studied. The limitations and explanations should be clarified, which can contribute to the relation of air–water mixtures and a continuous phase analysis model.

Data availability

The raw data are available on request from the corresponding authors.

Received: 27 September 2021; Accepted: 6 January 2022
Published online: 27 January 2022

References

1. Brocchini, M. & Peregrine, D. H. The dynamics of strong turbulence at free surfaces. Part 1. Description. *J. Fluid Mech.* **449**, 225–254 (2001).
2. Ervine, D. A. Air entrainment in hydraulic structures: A review. *Proc. Inst. Civ. Eng. Water Marit. Energy* **130**, 142–153 (1998).
3. Falvey, H. T. *Air–Water Flow in Hydraulic Structures* (USBR Engrg. Monograph, No. 41, 1980).
4. Falvey, H. T. *Cavitation in Chutes and Spillways* (USBR Engrg. Monograph, No. 42, 1990).
5. Toombes, L. & Chanson, H. Air–water mass transfer on a stepped waterway. *J. Environ. Eng.* **131**, 1377–1386 (2005).

6. Valero, D. & Bung, D. B. Reformulating self-aeration in hydraulic structures: Turbulent growth of free surface perturbations leading to air entrainment. *Int. J. Multiph. Flow* **100**, 127–142 (2018).
7. Wood, I. R. Free surface air entrainment on spillways. In: *Proceeding of IAHR Hydraulic Structure Design Manual No. 4* (1991).
8. Hager, W. H. Uniform aerated chute flow. *J. Hydraul. Eng.* **117**, 528–533 (1991).
9. Chanson, H. & Toombes, L. Air–water flows down stepped chutes: Turbulence and flow structure observations. *Int. J. Multiph. Flow* **28**, 1737–1761 (2002).
10. Wood, I. R. Air entrainment in high speed flows. In: *Proceeding of Scale Effects in Modelling Hydraulic Structures, IAHR* (1984).
11. Valero, D. & Bung, D. B. Development of the interfacial air layer in the non-aerated region of high-velocity spillway flows. Instabilities growth, entrapped air and influence on the self-aeration onset. *Int. J. Multiph. Flow* **84**, 66–74 (2016).
12. Straub, L. G. & Anderson, A. G. Experiments on self-aerated flow in open channels. *J. Hydraul. Div.* **84**, 1–35 (1958).
13. Wilhelms, S. C. & Gulliver, J. S. Bubbles and waves description of self-aerated spillway flow. *J. Hydraul. Res.* **43**, 522–531 (2005).
14. Dhillon, N., Buongiorno, J. & Varanasi, K. Critical heat flux maxima during boiling crisis on textured surfaces. *Nat. Commun.* **6**, 8247 (2015).
15. Hohermuth, B., Kramer, M., Felder, S. & Valero, D. Velocity bias in intrusive gas–liquid flow measurements. *Nat. Commun.* **12**, 4123 (2021).@@@
16. Deane, G. B. & Stokes, M. D. Scale dependence of bubble creation mechanisms in breaking waves. *Nature* **418**, 839–844 (2002).
17. Felder, S. & Chanson, H. Phase-detection probe measurements in high-velocity free-surface flows including a discussion of key sampling parameters. *Exp. Therm. Fluid Sci.* **61**, 66–78 (2015).
18. Felder, S. & Chanson, H. Air–water flow characteristics in high-velocity free-surface flows with 50% void fraction. *Int. J. Multiph. Flow* **85**, 186–195 (2016).
19. Zhang, G. & Chanson, H. Self-aeration in the rapidly and gradually varying flow regions of steep smooth and stepped spillways. *Environ. Fluid Mech.* **1**, 1–20 (2015).
20. Wei, W., Xu, W., Deng, J., Tian, Z. & Zhang, F. Analysis on link between the macroscopic and microscopic air-water properties in self-aerated flows. *China Ocean Eng.* **32**, 614–623 (2018).
21. Prandtl, L. Bericht über untersuchungen zur ausgebildeten turbulenz. *Z. Angew. Math. Mech.* **5**, 136–139 (1925) **(in Germany)**.
22. Wood, I. R. Uniform region of self-aerated flow. *J. Hydraul. Eng.* **109**, 447–461 (1983).
23. Chanson, H. Self-aerated flows on chutes and spillways. *J. Hydraul. Eng.* **119**, 220–243 (1993).
24. Cartellier, A. Simultaneous void fraction measurement, bubble velocity, and size estimate using a single optical probe in gas–liquid two-phase flows. *Rev. Sci. Instrum.* **63**, 5442–5453 (1992).
25. Murai, Y., Oishi, Y., Takeda, Y. & Yamamoto, F. Turbulent shear stress profiles in a bubbly channel flow assessed by particle tracking velocimetry. *Exp. Fluids* **41**, 343–352 (2006).
26. Kawase, Y. & Moo-Young, M. Correlations for liquid-phase mass transfer coefficients in bubble column reactors with Newtonian and non-Newtonian fluids. *Can. J. Chem. Eng.* **70**, 48–54 (1992).
27. Yuan, Z. & Michaelides, E. E. Turbulence modulation in particulate flows—A theoretical approach. *Int. J. Multiph. Flow* **18**, 779–785 (1992).
28. Kenning, V. M. & Crowe, C. T. On the effect of particles on carrier phase turbulence in gas-particle flows. *Int. J. Multiph. Flow* **23**, 403–408 (1997).
29. Rashidi, M., Hetsroni, G. & Banerjee, S. Mechanisms of heat and mass transport at gas–liquid interfaces. *Int. J. Heat Mass Transf.* **34**, 1799–1810 (1991).
30. Orlins, J. J. & Gulliver, J. S. Dissolved gas supersaturation downstream of a spillway. Part II: Computational model. *J. Hydraul. Res.* **38**, 151–159 (2000).
31. Politano, M., Amado, A. A., Bickford, S., Murauskas, J. & Hay, D. Evaluation of operational strategies to minimize gas supersaturation downstream of a dam. *Comput. Fluids* **68**, 168–185 (2012).
32. Politano, M., Castro, A. & Hadjerioua, B. Modeling total dissolved gas for optimal operation of multireservoir systems. *J. Hydraul. Eng.* **143**, 04017007 (2017).
33. Pope, S. B. *Turbulent Flows* (Cambridge University Press, 2000).
34. Crowe, C. T., Schwarzkopf, J. D. & Sommerfeld, M. *Multiphase Flows with Droplets and Particles* (CRC Press, 2012).
35. Dey, S. *Fluvial Hydrodynamics* (Springer Nature, 2014).
36. Brennen, C. E. *Fundamentals of Multiphase Flows* (Cambridge University Press, 2005).
37. Cain, P. *Measurements Within Self-Aerated Flow on a Large Spillway*. PhD thesis, University of Canterbury (1978)
38. Wei, W., Xu, W., Deng, J., Tian, Z. & Zhang, F. Experimental study of air–water interface properties in self-aerated flows. *J. Hydrodyn.* **31**, 940–948 (2019).
39. Xi, R. Z. Characteristics of self-aerated flow on steep chutes. In: *Proceeding of Hydraulics for High Dams, IAHR* (1988).
40. Pfister, M. & Hager, W. H. Self-entrainment of air on stepped spillways. *Int. J. Multiph. Flow* **37**, 99–107 (2011).
41. Chanson, H. (ed.) *Energy Dissipation in Hydraulic Structures (IAHR Monograph)* (CRC Press, 2015).
42. Anderson, A. G. *The Distribution of Air in Self-Aerated Flow in a Smooth Open Channel*, Report No. 48, St Anthony Falls Hydraulic Laboratory, University of Minnesota (1955).
43. Killen, J. M. *The Surface Characteristics of Self-Aerated Flow in Steep Channels*. PhD thesis, University of Minnesota (1968).
44. Kramer, M., Hohermuth, B., Valero, D. & Felder, S. Best practices for velocity estimations in highly aerated flows with dual-tip phase-detection probes. *Int. J. Multiph. Flow* **126**, 103228 (2020).

Acknowledgements

We gratefully thank the National Natural Science Foundation of China (Grant No. 51979183; 51939007) for financial support.

Author contributions

W.W. and J.D. initiated and performed concepts. W.W. worked on different facets of the data analysis and wrote the manuscript. J.D. conceived and supervised the work.

Competing interests

The authors declare no competing interests.

Additional information

Correspondence and requests for materials should be addressed to J.D.

Reprints and permissions information is available at www.nature.com/reprints.